Aerodynamic Optimization of the Nose Shape of a Train Using the Adjoint Method

J. Munoz-Paniagua[†], J. García, A. Crespo and F. Laspougeas

Grupo de Investigación de Mecánica de Fluidos aplicada a la Ingeniería Industrial, Universidad Politécnica de Madrid, C/José Gutiérrez Abascal 2, Madrid, 28006, Spain

†*Corresponding Author Email: le.munoz@upm.es*

ABSTRACT

The adjoint method is used in this paper for the aerodynamic optimization of the nose shape of a train. This method has been extensively applied in aircraft or ground vehicle aerodynamic optimization, but is still in progress in train aerodynamics. Here we consider this innovative optimization method and present its application to reduce the aerodynamic drag when the train is subjected to front wind. The objective of this paper is to demonstrate the effectiveness of the method, highlighting the requirements, limitations and capabilities of it. Furthermore, a significant reduction of the aerodynamic drag in a short number of solver calls is aimed as well. The independence of the computational cost with respect to the number of design variables that define the optimal candidate is stressed as the most interesting characteristic of the adjoint method. This behavior permits a more complete modification of the shape of the train nose because the number of design variables is not a constraint anymore. The information obtained from the sensitivity field permits determining the regions of the geometry where a small modification of the nose shape might introduce a larger improvement of the train performance. A good agreement between this information and the successive geometry modifications is observed here.

NOMENCLATURE

C_D	aerodynamic drag coefficient	X	vector of grid points coordinates
g	geometric constraint for objective function	x	vector of design variables
H	train height	y^+	wall unit
h	geometric relation between design variables	Δx^+	grid resolution in streamwise direction
		i	index for iteration in optimization process
J(x)	objective function	j	index for each objective function
N	Navier - Stokes equations	k	design variable index
U_∞	inlet velocity (train speed)	m	number of objective functions
u_τ	friction velocity	n	number of design variables
u	flow variables at discrete grid points	α_i	step size at iteration i
v	kinematic viscosity	λ^T	vector of adjoint variables

1. INTRODUCTION

High-speed trains are considered as one of the most efficient mean of transportation nowadays, and this situation has attracted much attention from researchers to still improve its performance. Lighter and faster trains have been developed, and a consequence of this evolution is the introduction of new aerodynamic problems that were neglected

before but now are notably significant. Thus, the aerodynamic optimization plays a key role in the design process of a high-speed train. Train aerodynamic problems are closely related to the flow around the vehicle. Over the past few years, this has led to extensive research in the analysis of the flow characteristics in many different scenarios. (Cheli *et al*. 2010), (Diedrichs *et al*. 2008), (Hemida and Baker 2010), (Krajnovic *et al*. 2012) or (Sun *et*

al. 2012) are only a short representation of all the references available in this field. Once the flow structures are pictured, it is possible to propose a geometric modification that can improve the aerodynamic performance of trains. Dealing with these optimization problems has traditionally been done by a trial-and-error procedure, which is very expensive in terms of computer and designer time. Furthermore, this procedure strongly depends on the expertise of the engineer. Advanced optimization algorithms try to use the information extracted from these previous analyses while, at the same time, present a new strategy to solve the problem based in a more automated fashion. The application of these methods is very popular in aircraft or vehicle aerodynamics, but is still in progress in train aerodynamics. Krajnovic (2009), Krajnovic *et al.* (2012), Vytla (2011) or Muñoz-Paniagua *et al.* (2011) resolve different single-objective optimization problems in open air using genetic algorithms (GA) and a geometric parameterization of two, five and ten design variables respectively. (Orellano 2010) considers the drag-crosswind multi-objective optimization problem for a sixty-design-variables nose shape parameterization and GA. (Jakubek and Wagner 2012) considers adjoint methods for the minimization of the pressure pulse generated by passing the train head. In the case of trains in tunnels, the optimization of the nose shape using new optimization methods is accomplished in Lee and Kim (2008) or Kwon *et al.* (2011), while (Muñoz-Paniagua *et al.* 2014) optimizes the nose shape to reduce the maximum pressure gradient at the entry of the tunnel using GA. Therefore, the interest of aerodynamic shape optimization for high-speed trains and the development and application of advanced optimization methods for train aerodynamics is evident.

Among the different options available, we have chosen the adjoint methods as the optimization tool for reducing the aerodynamic drag on the nose of a high-speed train subjected to front wind. GA is very popular in the aerodynamic optimization field, but their computational cost is directly related to the number of design variables used to parameterize the geometry of any optimal candidate. Moreover, the achievable improvement depends on the choice of the geometry parameters, (Othmer and Grahs 2005). As a consequence, a compromise between a robust and flexible geometric parameterization and an affordable computational effort is necessary, which is still more critical as the complexity of the flow simulation increases. The adjoint method is a gradient-based approach in which the calculation of the sensitivities is independent of the number of design variables, what results into a considerable time and computational cost saving. This removes the constraint normally set by dimensionality of the design space, where now every point on the train surface can be considered as a design variable. In fluid dynamics, the first reference of adjoint equations for design is given in Pironneau (1974), and more popularity was gained with the publications of Jameson, Jameson (1988) and Jameson and Martinelli (1998). Numerous publications on adjoint-based shape optimization

referred to external aerodynamics, Mohammadi and Pironneau (2004), Nadarajah (2003), Petropoulou (2010) or Reuther *et al.* (1996), stress the relevance of this technique. An overview of more applications of adjoint-based design is given in Mohammadi and Pironneau (2001) and Soto *et al.* (2004). In most of the previous references, the formulation of the adjoint approach is set in in-house code or in the open source solver OpenFOAM, while the implementation of the adjoint methods in commercial code is still very limited. To our knowledge, only AVL-FIRE, ESI-PAMFlow and ANSYS-FLUENT do include an adjoint solver. An application of the former is presented in Othmer (2006), where the shape optimization of a Volkswagen Golf car is developed. Here we use the ANSYS- FLUENT adjoint-solver to optimize the shape of the nose of a high-speed train subjected to front wind. Thus, our study is one of the first applications of adjoint methods to the aerodynamic optimization of high-speed trains using a commercial code. Nevertheless, we propose a slightly different optimization work-flow to the one embedded in the software. This new work-flow includes a CAD software which imports the proposed deformed geometry, so that it generates the new optimal candidate and exports it to be accurately meshed. Apart from the analysis of the effectiveness of the optimization methodology itself, it is obvious to highlight the interest of the analysis of the successive optimal candidates and the optimal solution. The reduction of the aerodynamic drag observed within this optimization method is significant enough to confirm the relevance of our research.

1.1 The Scope of the Study

These observations, the former optimization studies and the increasing importance of this new optimization method let us propose the following points.

1. Although the adjoint method has already been considered in many different applications, the complexity of the mathematical formulation and the limitations of the adjoint approach are identified as the reasons why this optimization method has not reached a still further popularity in the aerodynamics field (Giles 2000). The advantage of using a commercial code where the adjoint method is already implemented is presented in this paper, what might encourage other researchers for its application.

2. The adjoint method is not exactly novel, but the use of this in the aerodynamic optimization of high-speed trains is very recent. We use the discrete implementation of the adjoint method to optimize the nose shape of a smooth model of the leading control unit of the ICE 2, subjected to front wind. This geometry is known as the Aerodynamic Train Model (ATM), and the choice is based on the popularity and wide acceptance of it as a reference geometry among the train aerodynamics community. No publications are cited in the last annual review of heavy vehicles (Choi 2014) and, to our knowledge, our paper is the first case where the

minimization of the aerodynamic drag of an actual train using a commercial discrete implementation of the adjoint method is achieved. A description of the requirements, limitations and capabilities for this particular problem is included here.

3. Nevertheless, we propose a slightly different optimization work-flow to the one embedded in the software. This new work-flow includes a CAD software which imports the proposed deformed geometry, so that it generates the new optimal candidate and exports it to be accurately meshed. Even when the mesh morphing saves computational time during the optimization process, it is known that can have a negative impact on the quality of the mesh (Helgason 2012). Consequently, we ensure the grid independence in the optimization process.

4. Besides the discussion of the effectiveness of the optimization methodology itself, it is obvious to highlight the interest of the aerodynamic analysis of the successive optimal candidates and the optimal design. The flow field around the train head for the first and the final design is depicted in the paper.

The paper is organized as follows. A short description of the adjoint formulation is introduced in section 2. Section 3 is devoted to the methodology, where the work-flow and the numerical set-up are presented. The evolution of the shape of the nose is shown in section 4. Here a detailed description of the flow patterns and the modifications on the train shape are given, as well as the reduction of drag achieved during the optimization. Finally, the paper ends with a summary of the main conclusions.

2. DEFINITION AND FORMULATION OF THE PROBLEM

The objective of this study is the shape optimization of the nose of a high-speed train by minimizing its drag coefficient when it is exposed to a front wind. This single-objective optimization problem can be defined as

$$
\begin{array}{lll}
\text{Minimize} & J(\text{x}) & \\
\text{subject to} & g_j(\text{x}) \le 0 & j = 1 \dots m \\
& h_p(\text{x}) = 0 & l = 1 \dots s \\
& x_k^l \le x_k \le x_k^u & k = 1 \dots n
\end{array} \quad (1)
$$

where $J(\text{x})$ is the objective function (drag coefficient), and x is the vector of design variables that define the nose geometry. The inequality and equality constraints represent respectively constraints to be satisfied by the optimal candidate and relations between its design variables. If the optimal candidate at the iteration $i + 1$ is x_{i+1}, this can be defined based on a former design x_i as indicates (Vanderplaats 1984)

$$
\text{x}_{i+1} = \text{x}_i + \alpha_i \text{S}_i \quad (2)
$$

where α_i is the step size in the search direction S_i. Depending on how this search direction is defined, different optimization methods may be formulated.

If the search is based on evaluations of the objective function, zero-order methods are used, while if the first derivative of the objective function is used to obtain the gradient information, first-order methods are defined. The simplest way to define the search direction in the latter case is $\text{S}_i = - \nabla J(\text{x}_i)$, and the gradient is calculated via finite differences

$$
\frac{dJ}{dx_k} = \left(\frac{J(x_k + \Delta x_k) - J(x_k)}{\Delta x_k} \right) k = 1 \dots n \quad (3)
$$

what means that the number of objective function evaluations is of the order of $O(n)$, where n is the number of design variables. To reduce the computational cost of calculating dJ/dx_k, an adjoint approach is introduced. The main characteristic of the adjoint methods is that the calculation is independent of the number of design variables and only requires two solver calls to complete the sensitivity analysis.

This feature is the mean reason why we choose this method for the present optimization problem. Indeed, when using GA, even with the construction of a metamodel that speeds up the optimization process, the number of simulations is larger than four times the number of design variables. Meanwhile, as it has been mentioned, the gradient calculation using finite differences implies a number of solver calls of the order of $O(n)$.

There are two different ways to use the adjoint methods in CFD, the continuous and the discrete approach. ANSYS-FLUENT adjoint solver adopts the discrete approach, as this is avoids possible problems with the implementation of the boundary conditions that might cause the adjoint models to become inadmissible for the chosen objective function. The whole formulation of the method is out of scope of this paper. A detailed derivation can be found in (ANSYS 2012) or (Othmer and Grahs 2005). Nevertheless, we consider opportune to include a brief description of it.

2.1 Discrete Adjoint Method Overview

Give a set of design variables x that control the geometry of the nose, and a set of flow variables at discrete grid points u, the minimization of the objective function, which in general depends not only on the design variables but also on the flow variables, $J(u(x), x)$, is subject to the constraint that the discrete governing equations, N $(u(x), x) = 0$, must be all satisfied. As it has been indicated, the minimization of J requires the computation of the gradient, so

$$
\frac{dJ}{dx_k} = \frac{\partial J}{\partial u}\frac{du}{dx_k} + \frac{\partial J}{\partial x_k} \quad (4)
$$

subject to

$$
\frac{\partial N}{\partial u}\frac{du}{dx_k} + \frac{\partial N}{\partial x_k} = 0 \quad (5)
$$

It is observed in Eq. (4) that the challenge of determining the sensitivity of the objective function with respect to the design variables is the fact that a change in the latter induces a change in the flow variables, which indirectly changes the objective function. The adjoint method provides a mechanism for eliminating the specific changes that happen in the flow whenever the design variables are modified. From Eq. (5), it is obtained that

$$\frac{du}{dx_k} = -\left[\left(\frac{\partial N}{\partial u}\right)^{-1}\frac{\partial N}{\partial x_k}\right] \qquad (6)$$

what, after substitution in Eq. (4) and regrouping, results into

$$\frac{dJ}{dx_k} = \frac{\partial J}{\partial u}\left(-\left[\left(\frac{\partial N}{\partial u}\right)^{-1}\frac{\partial N}{\partial x_k}\right]\right) + \frac{\partial J}{\partial x_k} = \qquad (7)$$

$$\left[-\frac{\partial J}{\partial u}\left(\frac{\partial N}{\partial u}\right)^{-1}\right]\frac{\partial N}{\partial x_k} + \frac{\partial J}{\partial x_k}$$

Introducing the Lagrange multiplier λ, the resulting calculation of the sensitivity of J is given as

$$\frac{dJ}{dx_k} = -\lambda^T\frac{\partial N}{\partial x_k} + \frac{\partial J}{\partial x_k} \qquad (8)$$

where λ^T is the vector of adjoint variables (Lagrange multipliers). λ^T is chosen to satisfy

$$\frac{\partial J}{\partial u} = \lambda^T\frac{\partial N}{\partial u} \qquad (9)$$

which is called the adjoint equation. The adjoint equation is defined by the current state of the flow and does not depend on x_k. In consequence, not a solver call for each design variable but just two solver calls are required, one for the primal flow solver and one for the adjoint equation solver, namely dual.

2.2 Surface Deformation and Smoothing

The smoothness and continuity of the surface of objective is important to obtain a reasonable result of numerical calculations. For this reason, we think it might be interesting to briefly comment the surface deformation and the smoothing strategy in the adjoint solver. More information about these tasks is included in (ANSYS 2012).

The adjoint sensitivity data is used to determine how to modify the train nose shape to improve the train performance. The strategy for deciding how to modify the shape is based on the gradient algorithm. The change to a design variable (the normal displacement of each and every nose surface mesh node) is made in proportion to the sensitivity of the aerodynamic drag with respect to that design variable. Being the sensitivity of the objective function with respect to the shape

$$dJ = \frac{\partial J}{\partial x_k^s}dx_k^s \qquad (10)$$

where x_k^s is the *s*-th coordinate of the *k*-th node in the mesh (note that the design variables are the nodes of the surface mesh, and so x_k is the *k*-th design variable or node), then

$$dx_k^s = c\frac{\partial J}{\partial x_k^s} \qquad (11)$$

provides the maximum adjustment of *J* for given L^2 norm of dx_k^s, where *c* is an arbitrary scaling factor. In regions where the sensitivity is high, small adjustments to the shape will have a large effect on the observable.

It is important to remark that the field $\partial J/\partial x_k^s$ can be noisy in certain cases. If the noisy field is used directly to modify a boundary shape using Eq. (10), then the modified surface can have many inflections. To assure the continuity of the surface of objective, the use of mesh morphing tools will smooth the sensitivity field. The mesh morphing tool is not only a smoother for the surface sensitivity field (and consequently for the boundary mesh distortion), but also provides a smooth deformation of the interior mesh. The latter effect is not used in our work-flow as it will be explained afterwards, but the former is critical for preserving the continuity and smoothness of the nose surface. While in (Jakubek and Wagner 2012) radial basis functions are used for the boundary mesh deformation (displacement of nodes), here Bernstein polynomials are considered. More information can be obtained in (ANSYS 2012).

3. METHODOLOGY AND NUMERICAL SET-UP

The methodology considered here to optimize the train nose using adjoint methods is represented in Fig. 1. The optimization process consists on determining the sensitivity of the objective function with respect to the design variables. This information permits obtaining a map across the train nose surface of the effect of modifying the design. A gradient method uses this map to determine where to modify the surface, see Eq. (10). If *X* is the vector of mesh nodes coordinates, which depends on the nose shape (namely the vector of design variables **x**), the adaptation is introduced at the mesh *X* (**x**) so that the nodes of the mesh are either stretched or contracted. In this way, when using the adjoint method, the actual design variables are the normal displacements of each and every of the train nose surface mesh nodes, and the final result is a deformation of the geometry.

The preprocesing and the operations aforementioned are run within ANSYS-FLUENT. The mesh morpher implemented in the software permits closing the loop and solving iteratively the optimization process. However, we observed that the convergence of the simulations was influenced by the quality of the deformed mesh, and after several iterations this quality had decreased considerably. Therefore, teh second role of the mesh morpher is not taken into account here and, at each optimization step, the deformed geometry is exported and re-constructed in CATIA before an accurate meshing is performed. The meshing

process does always follow the same methodology. In this way, we ensure the grid independence in the optimization.
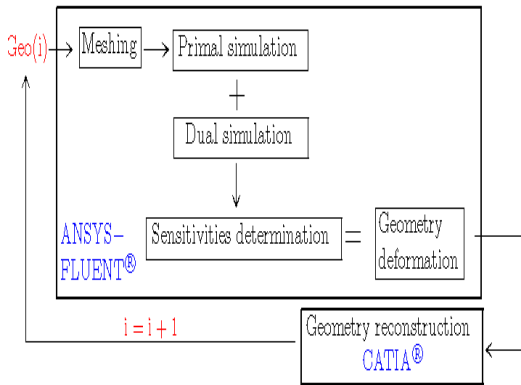

Fig. 1. Work-flow for the optimization process. Outside the default ANSYS-FLUENT workflow, we include the CAD software for the geometry reconstruction before remeshing the deformed geometry.

3.1 Train Geometry

The initial geometry to be optimized is a smooth model of the leading control unit of the Inter-City Express (ICE) 2. This is known as the Aerodynamic Train Model (ATM), and is widely accepted among the train aerodynamics community as a reference geometry Hemida and Krajnovic (2009) or Diedrichs (2008). Train elements like the pantograph, the bogies, the partial bogies skirts, the plough underneath the front-end or the inter-car gap are not included in the ATM model.

Only half a train is considered, and the tail of the train is not simulated. We extrude the car body cross-section to the end of the computational domain, so that we remove the need to treat the wake in the computation. Although a train operates with a symmetry in head and tail (*i.e.* the shape of the nose and the tail is the same), and we are aware of the significant contribution of the wake to the drag for bluff bodies, symmetry condition is not implemented in ANSYS-FLUENT 14.5. The adjoint solver permits to define just a single control volume where the geometry can be deformed, so the tail geometry will remain constant during the whole optimization process since the deformation is restricted to the volume around the train head. Consequently, to reduce the computational cost, subtracting this constant fraction of the total aerodynamic drag on the train, we limited the simulation to the front part of the train. Our decision is based on the usual procedure in train aerodynamic experimental studies, where a dummy end car is attached at the end of the leading control unit for wind tunnel tests, as many publications confirm, Orellano and Schober (2006) or Hemida and Krajnovic (2009). Indeed, in Raghunathan *et al.* (2002) a parametrical study of the aerodynamic behavior of the train shape is presented, and the experiments are run considering a reference tail. The high aspect ratio of the train, where its length is

greater than its height or width, suggests that the influence of the tail on the flow around the nose is negligible. Besides, it is known that in flows around configurations that have a predominant spatial direction, along which the mean properties of the flow field vary slowly, and have faster variations in span wise direction, simplified approaches may be applied in order to circumvent the large computational cost. Most of them are based on the parabolization of the flow equations, see Rubin and Tannehill (2004) and Paredes *et al.* (2012). Although this technique has not been directly used in this work, it indicates that the tail of the train has a small influence on the flow characteristics around the train head, thus justifying the optimization of its shape, independently of the rest.

3.2 Flow Domain and Boundary Conditions

The computational domain is represented in Fig. 2. The boundary conditions are also indicated there. The inlet is placed $11H$ upstream the train head, where H is the train height, the outlet is $5H$ far from the nose tip and the lateral walls are $7H$ far from the train longitudinal symmetry plane. The top is $9H$ from the ground. The domain boundaries do not interfere with the flow around the vehicle and are in good agreement with the European normative for numerical simulations of front wind (EN14067-4 2009). The flow direction is indicated by an arrow in Fig. 2. A constant velocity U_∞ = 50 m s^{-1}is used at the inlet of the computational domain. Although this velocity is not very high compared to actual high-speed trains, it is in the usual range of velocities used in other publications, and in particular this value was chosen to verify our results with Orellano and Schober (2006) or Raghunathan *et al.* (2002). Uniform pressure is imposed at the outlet, and symmetry condition is set at the sides and top of the domain. The ground is moving with U_∞ . The Reynolds number based on the inlet velocity and the train height is ~1.3×10^7.

3.3 Turbulence Model and Numerical Set-up

An incompressible, steady, turbulent flow simulation is considered. The standard k-ε turbulence model is used, with second order upwind momentum discretization scheme. The choice of this turbulence model is due to the fact that this model is the only one suported by the adjoint solver in ANSYS-FLUENT 14.5. Nevertheless, as zero yaw-angle is considered, not strong three-dimensional (3D) vortex shedding is expected as it would happen for large yaw angles. Therefore, it is acceptable the use of this turbulence model in this problem. Furthermore, the present paper focuses on the optimization method and the choice of an adequate method and the choice of the adequate turbulent model is left for future investigations standard wall functions implemented in the CFD software are used at the ground and on the train surface. $y^+ = u_\tau y/v$, where u_τ is the wall friction velocity and v is the kinematic viscosity of air, is fixed to 100. Δx^+ in terms of wall units y^+ is 25-250. A grid-independence analysis was performed, and the resulting computational mesh is given in Fig. 3.
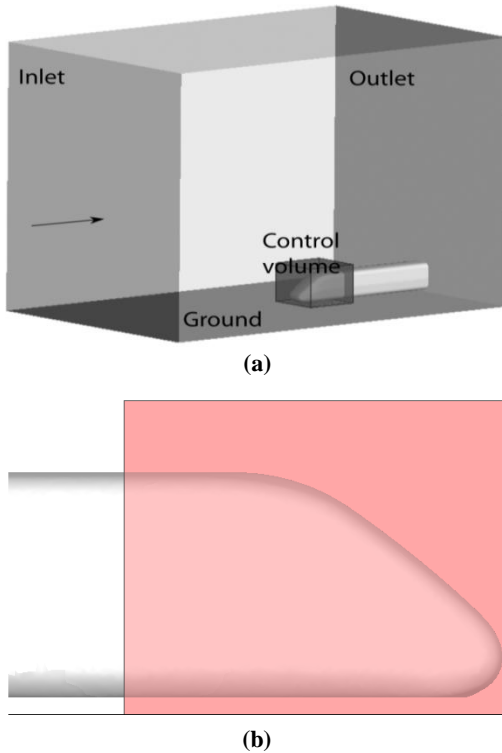
(a)

(b)

Fig. 2. a) Computational domain and boundary conditions. The flow direction is given by the arrow at the inlet of the domain. In b) a detail of the control volume is given. The tangency between the frontal face of the control volume and the nose tip is observed in this figure.
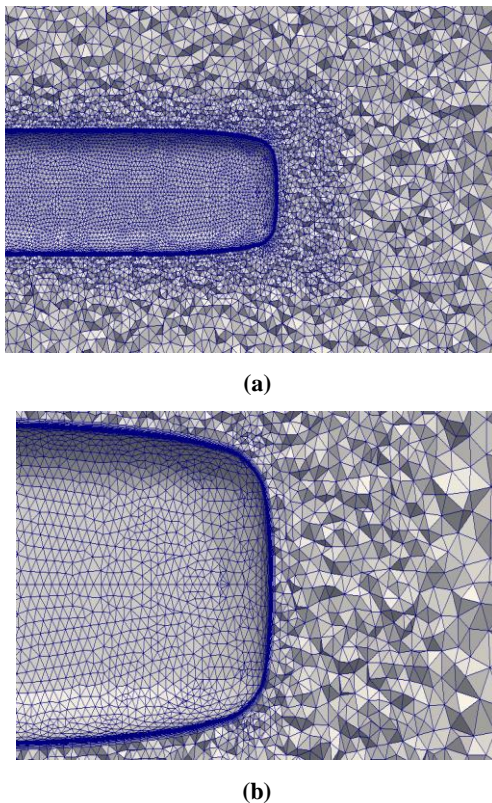

(a)

(b)

Fig. 3. Details of the mesh used for the numerical simulations

3.4 Adjoint Method Set-up

Related to the dual solver call, preconditioning is imposed. The Courant number is set to 0.1. The objective function with regard to the aerodynamic drag was computed just for the nose of the train because this is the train zone subject to modification. The scaling factor that controls the magnitude of the shape modification is 0.1. A rectangular control volume encloses the boundary whose shape is to be modified. The dimensions of this box are 6x5x5 m. In order to keep constant the nose length, the box is set tangent to the nose tip, see Fig. 2(b). In consequence, this point will be fixed. As the control volume intersects the car body, the cross-sectional area of the train is also kept constant. In this way, we ensure neither nose enlargement nor change of the car body frontal area.

4. ANALYSIS OF RESULTS

The solver is run initially without sensitivity updates to obtain a steady solution for both the primal and dual simulations of the original ATM train model. Then, the sensitivity information is used to introduce the first deformation of the nose shape. Six successive optimization steps are considered. Each of the geometries created is simulated until convergence. The evolution and reduction of the aerodynamic drag compared with the initial design are plotted in Fig. 4 The aerodynamic drag is defined as

$$C_D = \frac{D}{\frac{1}{2}\rho U_\infty^2 A} \tag{12}$$

where D is the drag force on the train nose (in Fig. 2 the control volume limits the train nose), ρ is the air density (1.225 kgm^{-3}) and A is chosen as 10 m^2, being this reference value given in the EN14067-4 (2009).
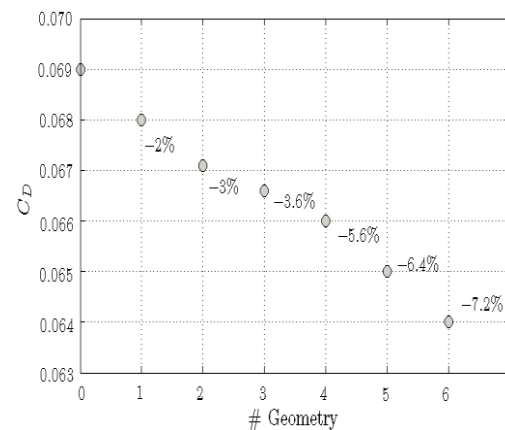

Fig. 4. Convergence history of the drag coefficient C_D

A reduction with respect to the ATM of 7.2 % is achieved. Our results of the initial geometry are in good agreement with the experimental results of the no-bogie-no-spoiler ATM geometry of Orellano and Schober (2006), although in this reference it is subtracted the volume corresponding to the bogies

from the train body, what explains the slight difference with our results. An experimental study of the nose length effect on the aerodynamic drag of the train is performed in Raghunathan (2002). In this reference, an inlet velocity of 50 m s^{-1} is used as well. The reduction of the aerodynamic drag when the nose is lengthened from $l/w = 1.0$ to $l/w = 2.0$, with l the nose length defined from the nose tip to the starting section of the carbody, and w the train width is of the same order of our optimization. $l/w = 2.0$ corresponds to our geometry #6, while a nose of $l/w = 1.0$ would be slightly shorter than our initial design. It is important to remark that a significant aerodynamic drag reduction is achieved within the fourteen solver calls compared to the computational cost of traditional optimization methods to achieve such improvement.

No convergence criteria as mesh quality degeneration is considered, because at each optimization step, the mesh is generated from scratch (although the same meshing strategy is adopted for all the cycles). The adjoint solver tool does not contemplate the possibility of introducing a volume restriction in order to avoid either unrealistic geometries. Therefore, even when reducing the aerodynamic drag, we adopted as a stop criteria of the optimization process when successive nose changes would evolve into a geometry that could not respect the volume required for the end coupler, the crash structure or the driver cabin (EN14067-4 2009).

The values of the drag coefficient are given for just the nose. The evolution of the geometry of the train nose is represented in Fig. 5 and Fig. 7. The lateral view and the top view are given for the successive six

optimization steps. The two-dimensional comparison of the nose profile helps the analysis of the nose profile evolution along the optimization process. It is observed that the extreme point of the nose is kept fixed, letting on one side the roof, windshield and hood, and on the other side the underbody to be modified. The control volume limits the displacement of the car body transition point in order to keep the nose length in the European standards of around 6 m length. In Fig. 6, the color map of the static pressure distribution on the surface of the original ATM geometry is given, and in the Fig. 7 the pressure distribution on the train surface for the six optimization steps is also plotted. The pressure range for Fig. 7 is the same as in Fig. 6. A large region of high positive pressure is observed at the nose tip, where the stagnation point is easily recognized. On the other hand, low negative pressure is visible at the transition between the nose and the car body, where the flow is accelerated. No flow detachment is observed, as it was expected. Nevertheless, this low negative pressure region is intended to be reduced. The lateral air flow around the A-pillars is accelerated and a low negative pressure distribution is observed in this region. Therefore, the geometry changes in the first iterations should aim to reduce the high positive pressure area at the nose tip while inducing

a more uniform pressure distribution all along the nose front.

These indications are observed in the next two iterations. The nose has been lengthened and the curvature of the roof has been modified so that the deflection of the flow has been reduced. Simultaneously, the bluntness of the nose has been decreased, shrinking the nose shape as it can be deduced from the top views of geometries #1 and #2. The high positive pressure at the nose tip has not been notably reduced because the shape of the nose tip remains constant. The consequence is the introduction of two bumps close to the tip.
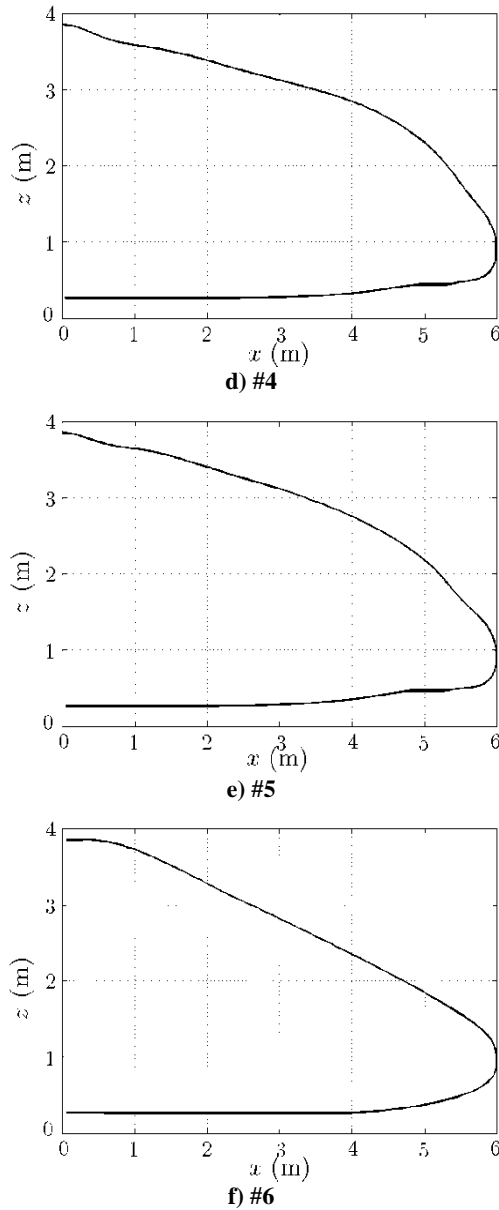

a) #1

b) #2

c) #3

d) #4

e) #5

f) #6
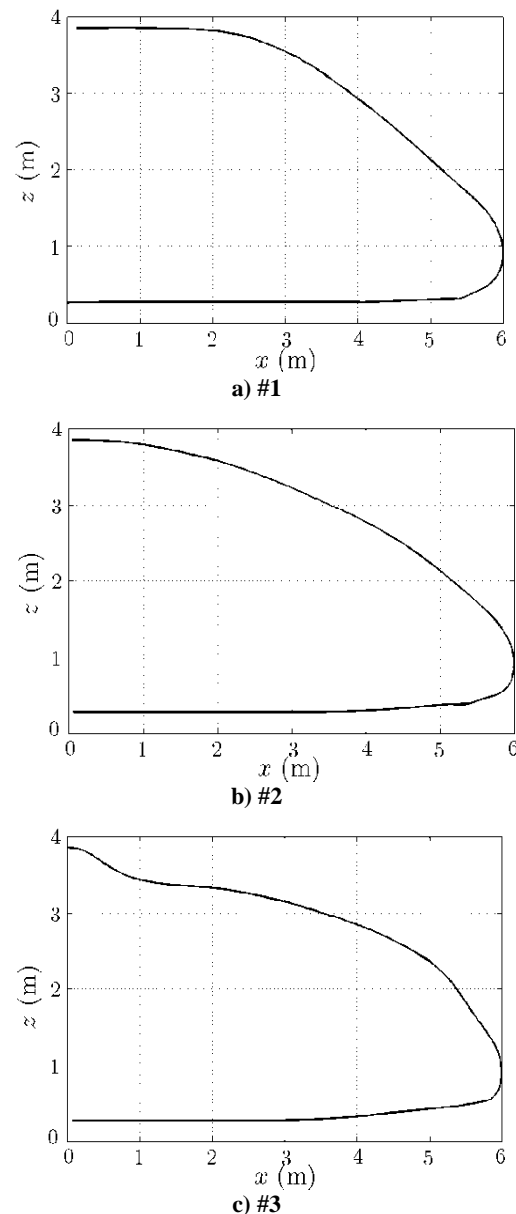
Fig.5. Lateral view of the nose shape for the successive geometries obtained within the optimization process

nose. Such hump is responsible of the positive pressure zone aforementioned while, at the same time, slightly extends the high pressure zone associated to the stagnation point and accelerates the flow along the hood.

The intensity of the hump is successively (#4 to #6) slowed down until a smooth nose profile is obtained. At the same time, the protuberances close to the nose tip are attenuated and the car body transition is softened.

The underbody has also been modified during the last iterations, resulting into an increase of the slope of the zone where the spoiler should be attached (in the following this region is called spoiler).
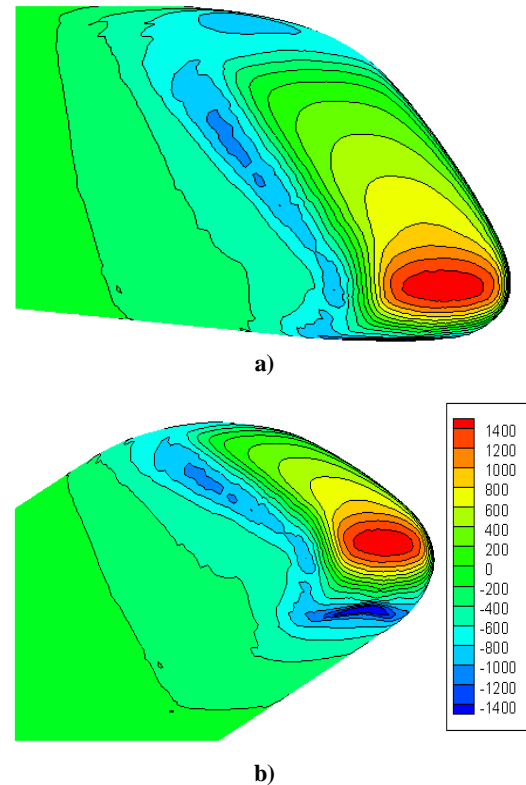

a)

b)

Fig. 6. Static pressure distribution on the surface of the ATM train model

The evolution to a slenderer nose is evident in the next step (#3). However, the restrictions imposed by the control volume, which fixes the cross-sectional area of the car body and the nose length, limit the changes. The tangency of the control volume with the tip of the train nose provokes that any deformation of the shape in the proximities of the tip is attenuated. Meanwhile, the intersection of the control volume and the car body imposes the original cross-sectional area to be kept constant and the result is a rough transition between the original car body and the deformed nose. The flow is more deflected and a positive pressure zone in the upper side of the train nose and a low pressure zone in the roof are observed. Another consequence of these restrictions and the evolution of the nose geometry is the introduction of a hump at the hood of the

This modification, with the lengthening of the train nose and the slenderness, follow the same tendency as in Orellano (2010), where a variation of the spoiler variation, a change in the car-body front transition and a more slender nose are introduced to reduce the aerodynamic drag of a high-speed train (other variations, like those concerning the bogie fairings are considered in this reference, but we do not, as bogies are not simulated in our train model).

In Fig. 8 a), the adjoint pressure or sensitivity to mass sources field for the initial geometry is represented. This field can be interpreted as the sensitivity of the observable with respect to mass sources or sinks in the domain, (ANSYS 2012). In other words, this field indicates the effect of

addition or removal of fluid from the domain upon the aerodynamic drag. Thus, we can translate this situation into the addition or removal of mass from the train and, therefore, the deformation of the train surface. The evolution of the nose shape previously described is confirmed by this sensitivity fields. If material were to systematically removed from the A-pillar and the top side where the transition between nose and car body takes place, then the drag will be reduced. In contrast, it is the addition of material to the nose tip that will induce a reduction of the aerodynamic drag. The addition of material to the nose tip can be expressed in terms of stretching the nose, so that the nose length increases and a slender train is obtained. Meanwhile, the removal of material at the train sides suggests to shrink the cross-sectional area along the train head, resulting into a sharper nose. Both effects are in good agreement with the basics of aerodynamics for bluff bodies, (Hucho 1993).

As it has been explained, the restriction that we impose makes impossible to stretch the nose because the control volume that encloses the surface object to be deformed is tangent to the nose tip. This point is then fixed, so no variation of the nose length is expected and the surface deformation is limited to the car body front transition zone and the A-pillar.

In Fig. 8 b), the same sensitivity field is plotted, but the geometry considered is \#5. In this case, negative sensitivity regions at the nose tip bumps (labeled as zone C) suggest that material needs to be removed from the train body to obtain a smoother design. At the same time, the hump observed at the nose hood has to be removed, so that the slope of the nose hood is reduced. The region between the car body transition and the window pane is colored in green, what suggests an addition of material. This region is located between two small bumps, (labeled as zone B) thus the conclusion is the necessity of stretching the former and shrinking the latter in order to obtain a smoother nose profile. The scaling factor is increased to 0.5 at this iteration to make more evident the geometry changes.

The train underbody can be observed in Fig. 9 a) and Fig. 9(b) for both geometries. Fig. 9(a) shows the necessity of removing material at the spoiler location, where a region of negative sensitivity is plotted (zone A). In contrast, in Fig. 9(b) it is not necessary anymore, but a deformation of the nose tip is still demanded, in order to reduce the bluntness of the nose.

5. CONCLUSION

Even when the adjoint method has already been considered in many different applications, the complexity of the mathematical formulation of the adjoint approach is one of the reasons why this optimization method has not reached a further popularity in the aerodynamics. Their independence with respect to the number of design variables makes them a very interesting option when dealing with a very large number of design variables. The

computational cost of each optimization iteration is of the order of $O(2)$, since just two solver calls are required, namely the primal and dual solver call. Therefore, the possibility of using this method implemented in a commercial code is very valuable. The method has been briefly introduced in this report, and the suitability of the adjoint method has been analyzed for the problem considered.

A reduction of a 7.2% of the aerodynamic drag in fourteen simulations (including those corresponding to the original design) has been obtained, and the evolution of the nose shape has been indicated in this paper. The high positive pressure region associated to the stagnation point has been reduced by designing a more slender nose. The nose length has been increased, and the slope of the windshield and hood has been decreased to avoid a larger flow detachment.

The information given by the sensitivity fields permit determine the regions of the geometry where a larger minimization of the aerodynamic drag can be achieved. This information is in good agreement with the resulting evolution of the nose shape all along the optimization process, and also is confirmed by the present tendency of new high-speed train designs and other optimization studies.

The most critical limitation observed when using the adjoint method is the difficulty of consider any geometrical constraint to avoid unrealistic geometries. The nose shape can change inside the control volume to minimize the objective function, but there is no way to limit this deformations so that a minimal volume or minimum dimensions are respected. Thus, future efforts should be directed to introduce geometrical constraints or a minimal reference geometry to be respected by all the optimal candidates. Another limitation is related to the control volume (an excessively large volume would difficult the convergence of the adjoint variables while a small volume would restrict many degrees of freedom). The deformation of the original mesh due to a change in the nose shape is also an important limitation to be considered during the optimization process. A good mesh-morphing tool would avoid re-meshing at each optimization step. However, it has been observed that even if small changes of the nose shape are introduced at each iteration, after a large number of iterations, the mesh is unavoidably distorted so much that this behavior directly affects the convergence of the numerical simulations. More improvements should be introduced concerning this point, as well as permitting compressible or unsteady simulations.

Nevertheless, the adjoint method still results into a very interesting tool when dealing with a large number of design variables, and the feature of not requiring a parameterization of the geometry is an excellent advantage that facilitates the optimization process. In the future, the application of the adjoint method in more located elements of the train (spoiler, bogie fairing or pantograph) could be considered. The minimization of the side force on

the nose and tail for cross-wind is also a possible optimization problem to be taken into account.

a) #1

b) #2
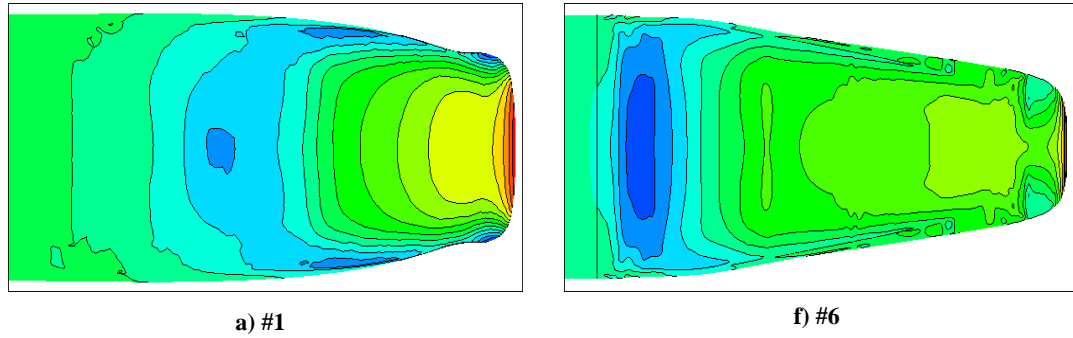

c) #3

d) #4

e) #5

f) #6

Fig. 7. Top view of the nose shape and color map of the static pressure distribution on the train surface for the successive geometries obtained within the optimization process
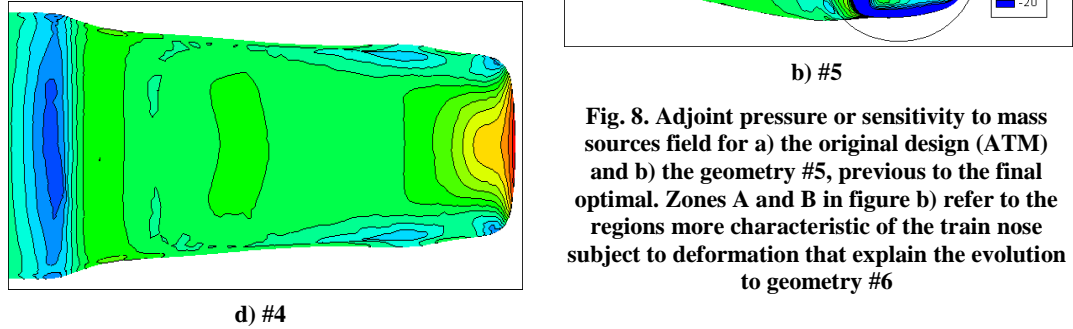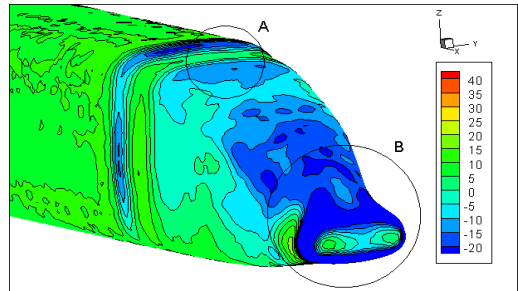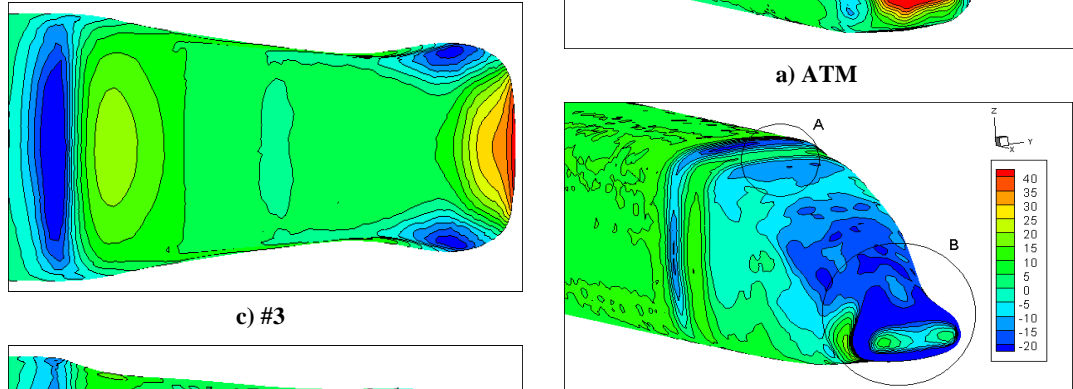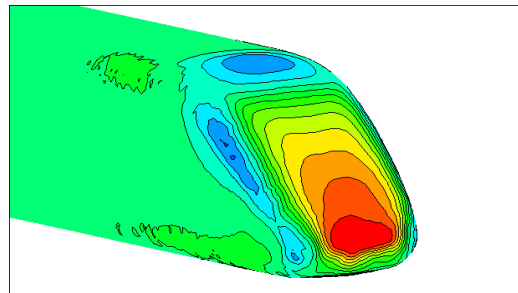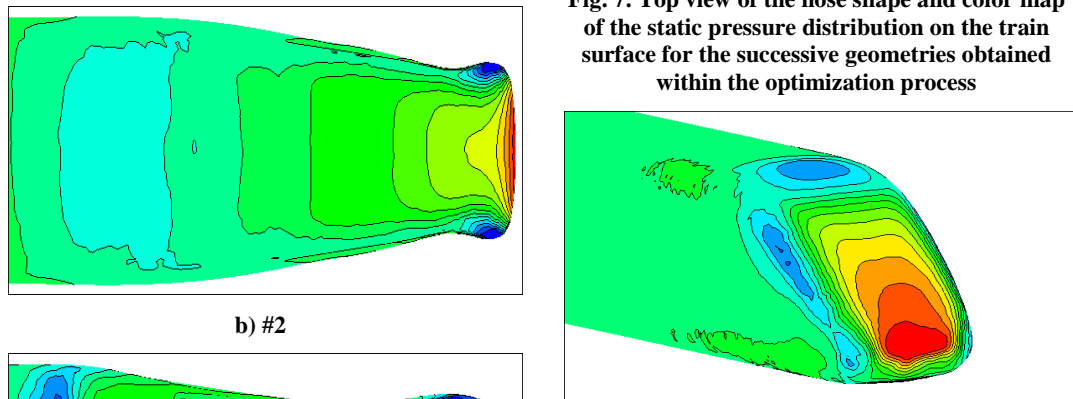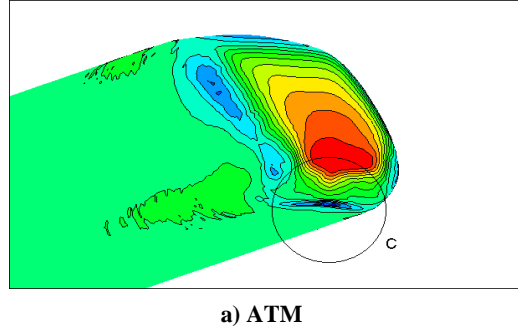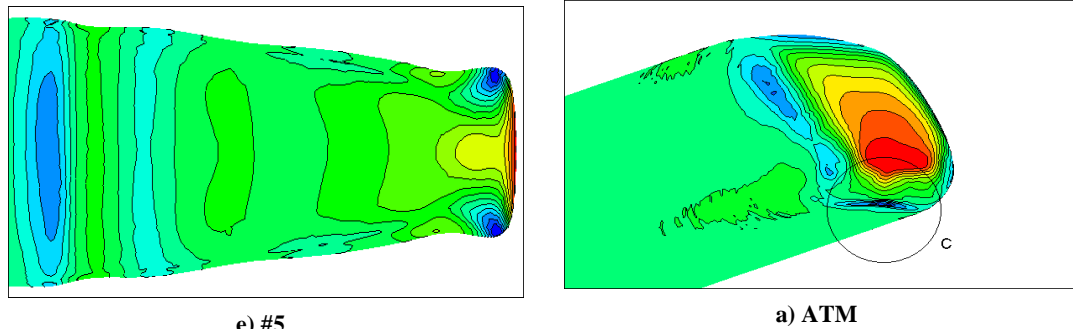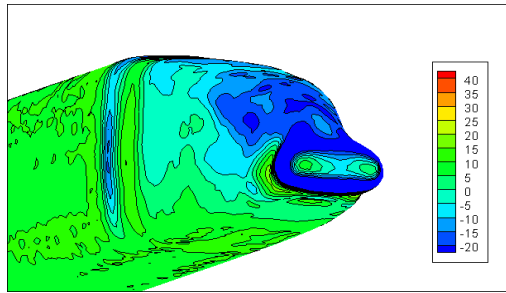

a) ATM

b) #5

Fig. 8. Adjoint pressure or sensitivity to mass sources field for a) the original design (ATM) and b) the geometry #5, previous to the final optimal. Zones A and B in figure b) refer to the regions more characteristic of the train nose subject to deformation that explain the evolution to geometry #6

a) ATM

b) #5

Fig. 9. Detail of the adjoint pressure or sensitivity to mass sources field on the underbody for both a) the original design (ATM) and b) the geometry #5, previous to the final optimal.

REFERENCES

ANSYS (2012). *ANSYS FLUENT Adjoint Solver. Release 14.5*. ANSYS Inc.

Cheli, F., F. Ripamonti, D. Rocchi, and G. Tomasini (2010). Aerodynamic behavior investigation of the new EMUV250 train to crosswind. *Journal of Wind Engineering and Industrial Aerodynamics* 98, 189-201.

Choi, H., J. Lee, and H. Park (2014). Aerodynamics of Heavy Vehicles, *Annu. Rev. Fluid Mech.* 46, 441-468.

Diedrichs, B. (2008). Aerodynamic calculations of crosswind stability of a high-speed train using control volumes of arbitrary polyhedral shape. *In BBAA VI International Colloquium on Bluff Bodies Aerodynamics & Applications,* Milano, Italy.

Diedrichs, B., S. Krajnovic, and M. Berg, (2008). On the Aerodynamics of Car Body Vibrations of High-speed Trains Cruising inside Tunnel. *Engineering Applications of Computational Fluid Mechanics* 2(1), 51-75.

EN14067-4 (2009). EN14067-4:2005+A1. Railway Applications - Aerodynamics - Part 4: Requirements and Tests Procedures for Aerodynamics on Open Track. BSI, 2005.

Giles, M. B. and N. A. Pierce (2000). An Introduction to the Adjoint Approach to Design. *Flow, Turbulence and Combustion* 65, 393-415.

Hemida, H. and C. Baker (2010). Large Eddy Simulation of the Flow around a Freight Wagon subjected to Crosswind. *Computers and Fluids* 39, 1944-1956.

Hemida, H. and S. Krajnovic (2009). Exploring Flow Structures around a Simplified ICE2 Train subjected to a 30° Side Wind using LES. *Engineering Applications of Computational Fluid Mechanics* 3(1), 28-41.

Hemida, H. and S. Krajnovic (2010). LES Study of the Influence of the Nose Shape and Yaw Angles on Flow Structures around Trains. *Journal of Wind Engineering and Industrial Aerodynamics* 98, 34-46.

Hucho, W. and G. Sovran (1993). Aerodynamics of Road Vehicles. *Annual Review of Fluid Mechanics* 25, 485-537.

Jakubek, D. and C. Wagner (2012). Shape Optimization of Train Head Cars using Adjoint-based Computational Fluid Dynamics. *International Journal of Railway Technology* 1(2), 67-88.

Jameson, A. (1988). Aerodynamic Design via Control Theory. *Journal of Scientific Computing* 3(3), 233-260.

Jameson, A. and L. Martinelli (1998). Optimum Aerodynamic Design using the Navier-Stokes Equations. *Theoretical and Computational Fluid Dynamics* 10, 213-237.

Krajnovic, S. (2009). Optimization of Aerodynamic Properties of High-speed Trains with CFD and Response Surface Models. In *The Aerodynamics of Heavy Vehicles II: Trucks, Buses and Trains, Volume 41 of Lecture Notes in Applied and Computational Mechanics*, 197-211, Springer Berlin - Heidelberg.

Krajnovic, S., E. Helgason, and H. Hafsteinsson (2012). Aerodynamic Shape Optimization of High-speed Trains. *In Proceedings of the First International Conference on Railway Technology: Research, Development and Maintenance*. Las Palmas de Gran Canaria, Spain.

Krajnovic, S., P. Ringqvist, K. Nakade, and B. Basara (2012). Large Eddy *Simulation* of the Flow around a Simplified Train moving through a Crosswind Flow. *Journal of Wind Engineering and Industrial Aerodynamics* 110, 86-99.

Kwon, H. -B., K. -H. Jang, Y. -S. Kim, K. -J. Yee, and D.-H. Lee (2001). Nose Shape Optimization of High-speed Train for Minimization of Tunnel Sonic Boom. *JSME International Journal Series C* 44(3), 890–899.

Lee, J. and J. Kim (2008). Approximate Optimization of High-speed Train Nose Shape for Reducing Micropressure Wave. *Structural

and Multidisciplinary Optimization 35(1), 79– 87.

Mohammadi, B. and O. Pironneau (2001). *Applied Shape Optimization for Fluids*. Oxford University Press.

Mohammadi, B. and O. Pironneau (2004). Shape Optimization in Fluid Mechanics. *Annual Review of Fluid Mechanics* 36, 255– 279.

Munoz-Paniagua, J., J. Garcia, and A. Crespo (2011). Aerodynamic Optimization of High-speed Train Nose using a Genetic Algorithm and Artificial Neural Networks. In *CFD and Optimization, an ECCOMAS Thematic Conference*. Antalya, Turkey.

Munoz-Paniagua, J., J. Garcia, and A. Crespo (2014). Genetically Aerodynamic Optimization of the Nose Shape of a High-speed Train entering a Tunnel. *Journal of Wind Engineering and Industrial Aerodynamics,* 130, 48-61.

Nadarajah, S. K. (2003). *The Discrete Adjoint Approach to Aerodynamic Shape Optimization.* Ph. D. Thesis, Stanford University.

Official Journal of the European Communities (2006). TSI-Technical Specification for Interoperability of the Trans-European High-speed Rail System. *Official Journal of the European Communities.*

Orellano, A. (2010). Aeroefficient - Optimized train. In *modeFRONTIER International Users Meeting* 2010, Trieste, Italy.

Orellano, A. and M. Schober (2006). Aerodynamic Performance of a Typical High-speed Train. In *4th WSEAS International Conference on Fluid Mechanics and Aeronautics.* Elounda, Greece

Othmer, C. (2006, September). CFD Topology and Shape Optimization with Adjoint Methods. In *VDI Fahrzeug- und Verkehrstechnik 13. Internationaler Kongress Berechnung und Simualtion im Fahrzeugbau*, Würzburg, Germany.

Othmer, C., and T. Grahs (2005). Approaches to Fluid Dynamic Optimization in the Car Development Process. In *6th International Conference on Evolutionary and Deterministic Methods for Design, Optimization and Control*

with Applications to Industrial and Societal Problems, EUROGEN 2005, Munich, Germany.

Paredes, P., V. Theofilis, and D. Rodríguez (2012). Parabolic Navier Stokes Solutions of Trailing Vortex Flows, *AIAA Paper 2012-3348*.

Petropoulou, S. (2010, June). Industrial Optimization Solutions based on OpenFOAM Technology. In *V European Conference on Computational Fluid Dynamics*, *ECCOMAS CFD*. Lisbon, Portugal.

Pironneau, O. (1974). On Optimum Design in Fluid Mechanics. *Journal of Fluid Mechanics* 64, 97–110.

Raghunathan, R. R., H. Kim, and T. Setoguchi (2002). Aerodynamics of high-speed railway train. *Progress in Aerospace Sciences* 38, 469– 514.

Reuther, J., A. Jameson, J. Farmer, L. Martinelli, and D. Saunders (1996). Aerodynamic shape optimization of complex aircraft configurations via an adjoint formulation. In AIAA Paper 96-0094.

Rubin, S. and J. Tannehill (2004). Parabolized/Reduced Navier Stokes Computational Techniques, *Annu. Rev. Fluid Mech*. 24, 117-144.

Soto, O., R. Lohner, and C. Yang (2004). An Adjoint-based Design Methodology for CFD Problems. *International Journal of Numerical Methods for Heat and Fluid Flow* 14(6), 734– 759.

Sun, Z., J. Song, and Y. An (2012). Numerical Simulation of Aerodynamic Noise Generated by High-speed Trains. *Engineering Applications of Computational Fluid Mechanics* 6(2), 173– 185.

Vanderplaats, G. N. (1984). *Numerical Optimization Techniques for Engineering Design: with Applications, Volume 32*. McGraw-Hill.

Vytla, V. V. (2011). Multidisciplinary Optimization Framework for High Speed Train using Robust Hybrid GA-PSO Algorithm. Ph. D. Thesis, Wright State University.